Letter Vol. 5, No. 5 / May 2018 / Optica 608

Quantum nonlinear light emission in metamaterials: broadband Purcell enhancement of parametric downconversion

Artur Davoyan[1,2] and Harry Atwater[1,3]

[1]Resnick Sustainability Institute, Kavli Nanoscience Institute, Department of Applied Physics and Materials Science, California Institute of Technology, 1200 E California Blvd. MC 128-95, Pasadena, California 91125, USA
[2]e-mail: davoyan@caltech.edu
[3]e-mail: haa@caltech.edu

Received 22 November 2017; revised 15 February 2018; accepted 13 April 2018 (Doc. ID 314042); published 14 May 2018

Single-photon and correlated two-photon sources are important elements for optical information systems. Nonlinear downconversion light sources are robust and stable emitters of single photons and entangled photon pairs. However, the rate of downconverted light emission, dictated by the properties of low-symmetry nonlinear crystals, is typically very small, leading to significant constraints in device design and integration. In this Letter, we study principles of spontaneous emission control (i.e., the Purcell effect) generalized to describe the enhancement of nonlinear generation of quantum light through spontaneous parametric downconversion. We develop a theoretical framework based on eigenmode analysis to study quantum nonlinear emission in a general anisotropic, dispersive, and lossy media. Our theory provides an unprecedented insight into the emission process. We find that spontaneous parametric downconversion in a media with hyperbolic dispersion is broadband and phase-mismatch-free. We further predict a significant enhancement of the downconverted emission rate in experimentally realistic nanostructures. Our theoretical formalism and approach to Purcell enhancement of nonlinear optical processes provides a framework for description of quantum nonlinear optical phenomena in complex nanophotonic structures.

OCIS codes: (160.3918) Metamaterials; (160.4330) Nonlinear optical materials; (190.4410) Nonlinear optics, parametric processes; (270.5580) Quantum electrodynamics; (270.1670) Coherent optical effects.

https://doi.org/10.1364/OPTICA.5.000608

The Purcell effect is an elegant manifestation of quantum engineering by which the spontaneous emission rates of individual quantum emitters can be dramatically altered [1,2]; see Figs. 1(a) and 1(b). Nonetheless, the complexity of emitter design and challenges associated with matching photon sources in frequency, polarization, and phase have to date limited the use of individual quantum emitters in quantum optical systems.

Nonlinear optical processes (e.g., spontaneous parametric downconversion [3] and four-wave mixing [4]) offer a distinctly different approach to light generation. Their relative simplicity, high single-photon indistinguishability, stability, and straightforward room-temperature entanglement make quantum nonlinear sources advantageous for a large variety of practical applications [5] as well as in benchmark quantum experiments [6]. However, sources based on quantum nonlinear processes suffer from a number of limitations, including phase mismatch, which constrains operation to a narrow, material-specific frequency band, and low efficiency (i.e., low photon pair generation rate per unit length), leading to bulky devices that do not lend themselves to compact monolithic integration [1]. We note that recent reports of waveguide-integrated structures can achieve high efficiency, but are typically at least 100 μm long [4,7–9] or utilize resonant cavities with very high quality factors [3,10,11]. Mitigating these constraints would enable high-efficiency quantum nonlinear sources of single and entangled photons for chip-scale optical devices.

Here, for the first time to the best of our knowledge, we reveal key insights of the spontaneous parametric downconversion in nonlinear metamaterials with hyperbolic dispersion. We show that by modifying light dispersion and the density of optical states in hyperbolic metamaterials, photon pair generation through spontaneous parametric downconversion may be enhanced over a broad frequency range. We develop a comprehensive theoretical formalism describing quantum nonlinear light emission in structures with a modified density of optical states, such as nonlinear metamaterials, highly dispersive crystals, and plasmonic nanostructures. We further identify new regimes of nonlinear light generation, including phase-mismatch-free, wavelength-tunable, and hyperbolic photon pair emission. Finally, we discuss experimental feasibility and design.

In spontaneous parametric downconversion, pump photons with frequency ω_p in a quadratically nonlinear crystal may spontaneously fission, shown in Fig. 1(c), to emit quantum-correlated signal and idler photons with frequencies ω_s and ω_i, respectively, and wavevectors $\boldsymbol{k}_s(\omega_s)$ and $\boldsymbol{k}_i(\omega_i)$, where energy conservation requires that $\omega_p = \omega_i + \omega_s$. The rate at which individual downconverted photons or photon pairs are generated is a key performance metric.

As is the case for ordinary spontaneous emission, shown in Figs. 1(a) and 1(b), spontaneous nonlinear luminescence depends on the strength of the quantum mechanical interaction and the density of available optical states in the system, $\rho \propto \int_{\partial\mathcal{V}_{\boldsymbol{k}}} |\frac{\partial\omega}{\partial \boldsymbol{k}}|^{-1} \mathrm{d}^2\boldsymbol{s}$(for an unbounded medium, where integration is over the isofrequency surface $\partial\mathcal{V}_{\boldsymbol{k}}$) [12]. However, spontaneous parametric downconversion also requires phase matching between the interacting pump, signal, and idler waves, $\Delta\boldsymbol{k} = \boldsymbol{k}_p - \boldsymbol{k}_s - \boldsymbol{k}_i \to 0$; see Fig. 1(c). Describing the Purcell-like enhancement of nonlinear luminescence requires modifying both the density of optical modes, determined by the isofrequency surface $\partial\mathcal{V}_{\boldsymbol{k}}$, and the light dispersion $\boldsymbol{k}(\omega)$ at the pump, signal, and idler wavelengths. We note that periodic poling of a nonlinear crystal helps to minimize the phase-matching constraint, but does not by itself significantly alter the density of optical states in the bulk of a nonlinear crystal [Fig. 1(d)]. The density of states can be tailored by using high-Q cavities and resonators as shown in Fig. 1(e), but this imposes a sensitive phase-matching requirement that reduces the downconversion bandwidth. By contrast, metamaterials designed with tailored subwavelength nanoscale structures can exhibit effective electromagnetic properties not readily available in nature. Nanophotonic materials with unusual material parameters have previously demonstrated the potential for nonlinear optical generation [13–16] and also for tuning radiation properties of isolated quantum emitters [17–19]. Reference [20] proposes a Green's function formulation to account for light emission in nonlinear metamaterials and applies this theory to study spontaneous four-wave mixing in hyperbolic metamaterials. In contrast to previous works, we develop here a conceptually different theoretical framework that is based on comprehensive eigenmode analysis to describe quantum nonlinear light emission in wide range of complex photonic systems. We further provide an in-depth insight into spontaneous parametric downconversion in metamaterials (Fig. 1) and discuss the ways to enhance and control these processes.

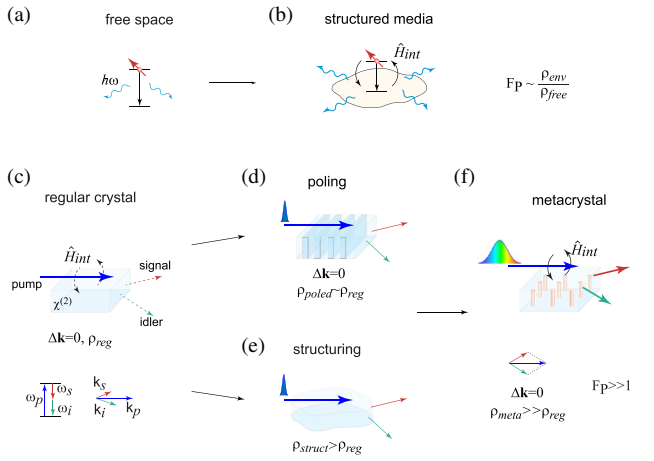

Fig. 1. Purcell enhancement of quantum nonlinear light generation with metamaterials. (a) An excited two-level system in free space decays by spontaneous emission. This process may be enhanced by modifying the emitter coupling to the photonic environment, (b). (c) Light may also be spontaneously emitted within a nonlinear crystal, when pump photons spontaneously fission, creating quantum-correlated signal-idler photon pairs. Nonlinear generation depends on the density of optical states, ρ_{reg}, and the strength of light–material interaction $\hat{H}_{\mathrm{int}}$, which also depends on phase matching between the pump, signal, and idler waves ($\Delta\boldsymbol{k}$)—a condition hard to meet in bulk nonlinear materials. (d) Poling of a crystal minimizes the phase mismatch ($\Delta\boldsymbol{k} \to 0$) for a spectrally narrow operation range, but in general the density of optical modes is not significantly changed ($\rho_{\mathrm{poled}} \simeq \rho_{\mathrm{reg}}$). (e) Modification of the density of optical states in a resonator or a waveguide enhances emission and modifies the phase-matching conditions, but the high quality factor limits the operational frequency range. (f) Conversely, metamaterials may enable nonresonant, broadband, phase-mismatch-free Purcell enhancement of spontaneous nonlinear light emission.

To illustrate the principles for modifying spontaneous downconversion with metamaterials, we consider a uniaxial crystal with an effective tensor permittivity $\bar{\bar{\varepsilon}} = \mathrm{diag}(\varepsilon_\perp, \varepsilon_\perp, \varepsilon_\parallel)$. Figure 2(a) shows the isofrequency surfaces for different variations of the ordinary ($\varepsilon_\perp$) and extraordinary ($\varepsilon_\parallel$) components of the permittivity tensor. For regular crystals ($\varepsilon_\parallel > 0$ and $\varepsilon_\perp > 0$), the isofrequency surfaces are ellipsoidal [Fig. 2(a)]. The closed topology of these surfaces implies that the density of optical modes is finite (i.e., $\int_{\partial\mathcal{V}_{\boldsymbol{k}}} |\frac{\partial\omega}{\partial \boldsymbol{k}}|^{-1} \mathrm{d}^2\boldsymbol{s} \ll \infty$). Phase matching occurs only for a certain finite range of pump wavevectors; see Fig. 3(a).

In metamaterials, a different regime can be accessed, where either $\varepsilon_\parallel < 0$ or $\varepsilon_\perp < 0$ [17,21]. This is possible, for instance, in alternating subwavelength metal–dielectric structures, as shown schematically in Fig. 3(d), or in bulk crystals with pronounced material resonances, e.g., hexagonal boron nitride and bismuth selenide [22]). In such materials, the isofrequency surfaces for extraordinary waves are transformed into hyperboloids [17,21]; see Fig. 2(a). Hence, a large optical mode density becomes accessible (ideally infinite, but in practice it is limited by losses and the achievable minimum period of the layered structure, i.e., $\max(|\boldsymbol{k}|) \simeq \frac{2\pi}{\Lambda}$). Open hyperbolic isofrequency dispersion surfaces, in contrast with regular dispersion surfaces, remove phase-matching constraints—that is, for any pump wavevector there is always a pair of signal-idler photons such that $\Delta\boldsymbol{k} = 0$ [see Figs. 3(c), 3(d), and 3(f), and a corresponding discussion in Supplement 1 (S2,S3)]. Phase-mismatch-free operation in the hyperbolic regime, as we show below, enables broadband operation.

From a simple phase-matching analysis, we can specify the preferred directions for single-photon emission. Conical emission is anticipated for conventional crystals, as shown in Fig. 3(a), and for hyperbolic metamaterials pumped along the crystal axis ($\boldsymbol{k}_p \| \boldsymbol{z}$) see Fig. 3(b). However, for a pump perpendicular to the metamaterial axis ($\boldsymbol{k}_p \| \boldsymbol{x}$), the expected light emission is hyperbolic,

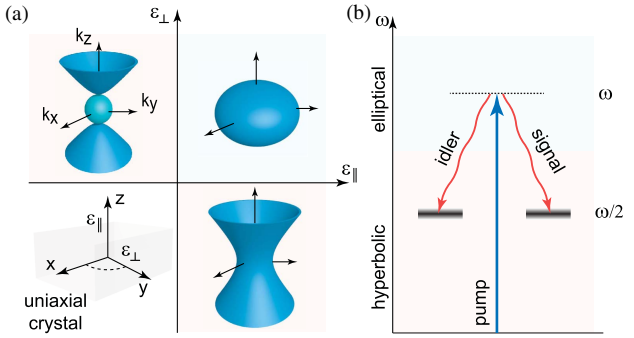

Fig. 2. (a) Map of possible isofrequency surfaces ($\partial\mathcal{V}_{\boldsymbol{k}}$) for a uniaxial crystal. Elliptical and hyperbolic dispersion regimes may be accessed by controlling the signs of ordinary, $\varepsilon_\perp$, and extraordinary, $\varepsilon_\parallel$, permittivities. Notably, a semi-infinite number of optical modes are available in materials with hyperbolic dispersion ($\rho \propto \partial\mathcal{V}_{\boldsymbol{k}}$). (b) Spectral diagram of the downconversion process treated here. The metamaterial is pumped in an elliptical dispersion regime, whereas spontaneous downconversion of the signal-idler pairs occurs in the hyperbolic dispersion regime. Color gradient depicts the expected fluorescence probability.

as shown in Figs. 3(c) and 3(d). We predict that it is this combination of phase-mismatch-free parametric downconversion together with a near-infinite number of available optical modes that leads to a substantial enhancement of signal-idler downconverted photon pair emission rate. (Note that a similar criterion is satisfied for some other spontaneous wave-mixing processes, e.g., spontaneous four-wave mixing [20]).

To probe the spontaneous parametric downconversion in the hyperbolic regime, we consider a process schematically shown in Fig. 2(b). We assume that photons of a pump laser beam in an elliptical dispersion regime spontaneously downconvert to extraordinary signal and extraordinary idler waves, both within a hyperbolic dispersion regime. To be specific, we consider a continuous plane-wave pump propagating along the $\boldsymbol{x}$ axis [as shown in Figs. 3(c) and 3(d)]. We develop a general quantum mechanical model that predicts the downconversion rate in a range of complex structures, including such extremely anisotropic uniaxial metamaterials [see Supplement 1 (S6) for a detailed discussion]. In contrast to previous works (e.g., Ref. [20]), our theory is based on the comprehensive eigenmode analysis, which enables a deeper insight to key physical process in a variety of complex systems. We find that the emitted signal photon spectral power density may be estimated as

$$\frac{dP_s}{d\lambda_s} = \frac{\hbar\pi c^3 L^2}{\lambda_s^4 \lambda_i} \frac{P_p}{\varepsilon_0 n_p} \times \int \mathrm{d}^2\boldsymbol{k}_{s\perp} c_{\boldsymbol{k}_s}^2 c_{\boldsymbol{k}_i}^2 \frac{\partial k_{s\parallel}}{\partial\omega}\frac{\partial k_{i\parallel}}{\partial\omega} N(\boldsymbol{k}_s) \left|\frac{1-e^{i\Delta\boldsymbol{k}L}}{i\Delta\boldsymbol{k}L}\right|^2 e^{-\gamma'(\boldsymbol{k}_s)L}, \quad (1)$$

where $N(\boldsymbol{k}_s) = |\sum \tilde{\chi}^{(2)}_{lmn} u_l(\omega_p) u_m(\omega_s) u_n(\omega_i)|^2$ corresponds to a nonlinear media "polarization mixing" term with $\tilde{\chi}^{(2)}$ being a nonlinear susceptibility and $\boldsymbol{u}_{p,s,i}$ corresponding to polarization of pump, signal, or idler waves; $\lambda_{s,i}$ are signal and idler wavelengths; P_p is the pump power in the crystal; n_p is effective index at the pump wavelength; $c_{\boldsymbol{k}_{s,i}}$ are the coefficients due to quantization of the interacting fields; $d^2\boldsymbol{k}_\perp = dk_{sy}dk_{sz}$ with k_{sy} and k_{sz} being y and z components of the signal wavevector $\boldsymbol{k}_s$; $\frac{\partial k_{s,i\parallel}}{\partial\omega}$ refer to group velocities of signal and idler waves in the direction of pump propagation; L is the propagation length; and $e^{-\gamma'(\boldsymbol{k}_s)L}$ is the quantum mechanical signal photon decay rate. In our analysis we consider an effective medium model [Supplement 1 (S2)] and take into account dispersion and losses perturbatively [Supplement 1 (S6)]; the validity of these assumptions is discussed in the Supplement 1.

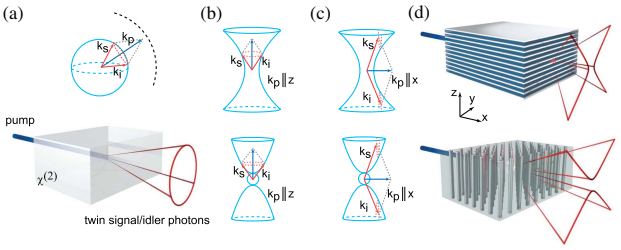

Fig. 3. (a) Phase-matching diagram and corresponding photon emission pattern for an isotropic medium. For this closed isofrequency manifold, phase matching is possible only for a limited range of pump wavevectors ($|\boldsymbol{k}_p| \le 2|\boldsymbol{k}_s|$). The dashed line denotes a condition beyond which phase matching is not possible. The photon emission is conical in this case. (b,c) Schematic of phase matching in layer- and wire-like hyperbolic metamaterials for pump propagation along the metamaterial axis. Open hyperbolic isofrequency surfaces for both of the hyperbolic cases imply pump wavevector-independent phase-mismatch-free operation. The light emission is conical, similar to the isotropic case in panel (a). (d) A phase-mismatch-free condition is also obtained for pump propagating along the $\boldsymbol{x}$ axis of the hyperbolic layer and wire metamaterials, respectively. However, in this case signal and idler waves encompass an infinitely large state space enabling a significant Purcell-like enhancement of nonlinear luminescence. Panel (d) shows the expected emission patterns in red for this pump propagation configuration.

We consider further, as an example, nonlinear parametric downconversion in metal–dielectric hyperbolic metamaterials whose dielectric components comprise a second-order nonlinear medium. Figures 4(a) and 4(b) show the power emission spectra calculated for silver (Ag)–lithium niobate ($LiNbO_3$) wire-like hyperbolic [Fig. 4(a)] and layered hyperbolic [Fig. 4(b)] metamaterials with 80 nm period and 25% metal filling fraction after $L = 500$ nm of propagation for 1 mW of input pump power. Note that in our analysis we consider real material parameters for both silver and nonlinear dielectric [see Supplement 1 (S1, S5)]. For both of the hyperbolic systems we observe strong nonlinear luminescence in a broad range of pump wavelengths ($\simeq$150 nm of operation bandwidth). The peak emitted signal spectral power density reaches 6 fW/nm for a layered hyperbolic metamaterial and 22 fW/nm for a wire-like hyperbolic metamaterial [see also Supplement 1 (S4)].

We estimate the rate of single-photon emission, R_{meta}, in a degenerate case (i.e., when $\lambda_s = 2\lambda_p$); see Fig. 4(c) and Supplement 1 (S1). Specifically, we predict 25,000 photons/s for layered metamaterials and 70,000 photons/s for wire-like metamaterials, respectively. To quantify the emission enhancement, we introduce a Purcell-like coefficient for parametric luminescence, $F = R_{\mathrm{meta}}(L)/R_{\mathrm{regular}}(L)$, where we compare the emission rate of our metamaterials with that of a regular unpoled bulk crystal after the same propagation length. For both wire-like and layered hyperbolic metamaterials, we obtain a nearly $F = 50$ times increase in luminescence intensity.

The influence of losses is studied in Fig. 4(d). A peak is clearly seen in emission at $L \simeq 500$ nm due to an interplay between the downconverted photon generation probability, which is proportional to interaction length L, and photon absorption, which varies as $e^{-\gamma'(\boldsymbol{k}_s)L}$. However even after 2–3 μm of propagation, the overall luminescence intensity remains reasonably high. A similar dynamics is expected for a pair coincidence rate, which would be proportional to the probability of observing both signal and idler photons that scales as $\sim e^{-(\gamma'(\boldsymbol{k}_s)+\gamma'(\boldsymbol{k}_i))L}$.

Our predictions may be extrapolated to other second-order materials with refractive indices and nonlinear responses similar to $LiNbO_3$ (the dominant component in $LiNbO_3$ is $d_{33} = 34.4$ pm/V ($\chi^{(2)}_{zzz} = 2d_{33}$) [23]). Hence, a nearly 3.5 times weaker signal is expected for a potassium titanyl phosphate (KTP) with $d_{33} = 18.5$ pm/V [24], whereas for some organic polymers, d_{33} values as high as $\simeq$100 pm/V were reported [25]; in this case an almost ninefold stronger effect is anticipated.

Finally, as an example of a different material system, we consider light generation in silver–gallium phosphide (GaP) metamaterials. Gallium phosphide is a high-refractive-index semiconductor compatible with silicon nanofabrication processes and demonstrating a strong second-order optical response [$d_{24} \simeq 100$ pm/V ($\chi^{(2)}_{xyz} = 2d_{24}$)] [23]. However, a significant material dispersion prevents the use of GaP in conventional practice, since the phase-matching conditions cannot be met in the bulk crystal. The high index and strong nonlinearity of GaP facilitate compact device integration and higher photon generation rates. Our calculations

predict a substantial luminescence at $\lambda_p = 400$ nm after only 50 nm of propagation (about 4 times that of the tenfold thicker $LiNbO_3$-based structures studied above and ≃1000 times stronger than for a homogeneous gallium phosphide film of the same thickness); see Fig. 4(e). We anticipate a generation rate of over 3×10^5 signal photons/s in this case [see inset in Fig. 4(e)]. The light emission pattern shown in Fig. 4(f) is hyperbolic, as is expected from our simple phase-matching considerations.

Our predictions of high luminescence intensities in submicron-thickness structures suggest that compact broadband nonlinear single-photon sources may be designed. We expect that the actual emission enhancement may differ slightly from our predictions due to potential fabrication imperfections and effects beyond the scope of our model (such as a finite pump beam size [12], limitations of the effective medium approach, and boundary effects of the quantization model).

To conclude, in our analysis we have developed a general framework to describe spontaneous nonlinear downconversion in complex three-dimensional metamaterials, taking into account photonic band structure, dispersion, and losses. We further predicted that in hyperbolic metastructures broadband, enhanced, and phase-mismatch-free generation of quantum light may be attained. We note that our theoretical formalism and conceptual approach could be easily extended to other photonic platforms (e.g., hyperbolic metasurfaces [26] and epsilon-near-zero metamaterials [14,18,19]) and other frequency domains (near and mid-infrared, where potentially highly nonlinear multi-quantum-well semiconductor heterostructures may be utilized [13,27]) as well as nonmetallic systems (such as all-dielectric near-zero-index crystals [28] and phonon-polariton systems [22]).

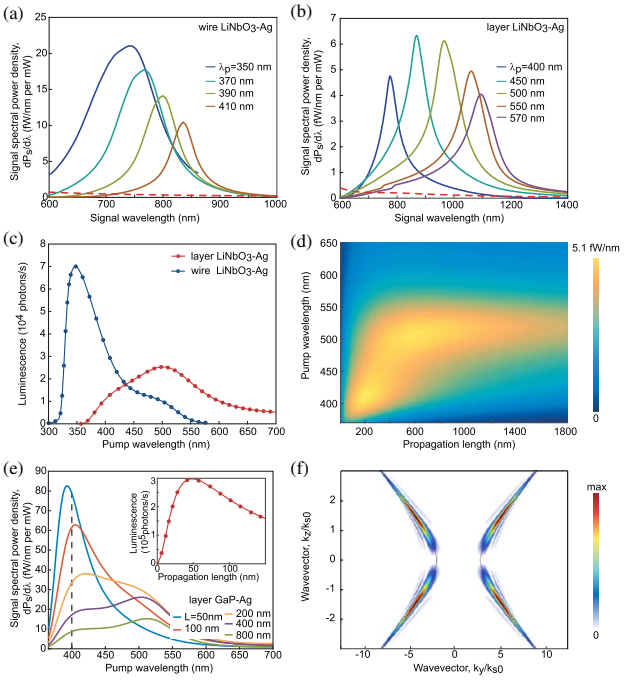

Fig. 4. (a) Calculated spectral power density of emitted signal photons for a wire-like hyperbolic $LiNbO_3$–Ag metamaterial for different pump wavelengths. The dashed curve shows expected emission from a bulk $LiNbO_3$ crystal of similar thickness at $\lambda_p = 350$ nm. (b) Spectral power density of emitted signal photons for a layer-hyperbolic metamaterial. The dashed curve shows the expected emission from a bulk $LiNbO_3$ at $\lambda_p = 500$ nm, for comparison. (c) Single-photon luminescence rate for frequency-degenerate downconversion (i.e., $2\lambda_p = \lambda_s = \lambda_i$) as a function of a pump wavelength for layered hyperbolic and wire-like hyperbolic $LiNbO_3$–Ag metamaterials. (d) Signal-photon spectral power density at the frequency-degenerate downconversion wavelength for a layered hyperbolic metamaterial as function of pump wavelength and propagation length. (e) Calculated signal photon spectral power density at the frequency-degenerate downconversion wavelength as a function of the pump wavelength for different propagation lengths for a layer-hyperbolic 70 nm GaP–30 nm Ag metamaterial. Inset shows the calculated luminescence for a 400 nm pump wavelength. (f) Signal photon emission map for a layer-hyperbolic GaP-Ag crystal at 400 nm pump wavelength after 500 nm of propagation.

Funding. Air Force Office of Scientific Research (AFOSR) (FA9550-16-1-0019).

See Supplement 1 for supporting content.

REFERENCES

1. M. D. Eisaman, J. Fan, A. Migdall, and S. V. Polyakov, Rev. Sci. Instrum. **82**, 071101 (2011).
2. P. Lodahl, S. Mahmoodian, and S. Stobbe, Rev. Mod. Phys. **87**, 347 (2015).
3. M. Fortsch, J. U. Fürst, C. Wittmann, D. Strekalov, A. Aiello, M. V. Chekhova, C. Silberhorn, G. Leuchs, and C. Marquardt, Nat. Commun. **4**, 1818 (2013).
4. J. W. Silverstone, D. Bonneau, K. Ohira, N. Suzuki, H. Yoshida, N. Iizuka, M. Ezaki, C. M. Natarajan, M. G. Tanner, R. H. Hadfield, V. Zwiller, G. D. Marshall, J. G. Rarity, J. L. O'Brien, and M. G. Thompson, Nat. Photonics **8**, 104 (2014).
5. A. Aspuru-Guzik and P. Walther, Nat. Phys. **8**, 285 (2012).
6. A. Aspect, J. Dalibard, and G. Roger, Phys. Rev. Lett. **49**, 1804 (1982).
7. S. Tanzilli, W. Tittel, H. De Riedmatten, H. Zbinden, P. Baldi, M. DeMicheli, D. B. Ostrowsky, and N. Gisin, Eur. Phys. J. D **18**, 155 (2002).
8. M. Fiorentino, S. M. Spillane, R. G. Beausoleil, T. D. Roberts, P. Battle, and M. W. Munro, Opt. Express **15**, 7479 (2007).
9. R. Horn, P. Abolghasem, B. J. Bijlani, D. Kang, A. S. Helmy, and G. Weihs, Phys. Rev. Lett. **108**, 153605 (2012).
10. D. Grassani, S. Azzini, M. Liscidini, M. Galli, M. J. Strain, M. Sorel, J. E. Sipe, and D. Bajoni, Optica **2**, 88 (2015).
11. Q. Li, M. Davanco, and K. Srinivasan, Nat. Photonics **10**, 406 (2016).
12. K. Koch, E. C. Cheung, G. T. Moore, S. H. Chakmakjian, and J. M. Liu, IEEE J. Quantum Electron. **31**, 769 (1995).
13. J. Lee, M. Tymchenko, C. Argyropoulos, P.-Y. Chen, F. Lu, F. Demmerle, G. Boehm, M.-C. Amann, A. Alù, and M. A. Belkin, Nature **511**, 65 (2014).
14. M. Z. Alam, I. de Leon, and R. W. Boyd, Science **352**, 795 (2016).
15. G. Marino, P. Segovia, A. V. Krasavin, P. Ginzburg, N. Olivier, G. A. Wurtz, and A. V. Zayats, Laser Photon. Rev. **12**, 1700189 (2018).
16. C. Duncan, L. Perret, S. Palomba, M. Lapine, B. T. Kuhlmey, and C. M. de Sterke, Sci. Rep. **5**, 8983 (2015).
17. H. N. S. Krishnamoorthy, Z. Jacob, E. Narimanov, I. Kretzschmar, and V. M. Menon, Science **336**, 205 (2012).
18. A. M. Mahmoud and N. Engheta, Nat. Commun. **5**, 5638 (2014).
19. R. Sokhoyan and H. A. Atwater, "Cooperative behavior of quantum dipole emitters coupled to a zero-index nanoscale waveguide," arXiv: 1510.07071 (2015).
20. A. N. Poddubny, I. V. Iorsh, and A. A. Sukhorukov, Phys. Rev. Lett. **117**, 123901 (2016).
21. C. L. Cortes, W. Newman, S. Molesky, and Z. Jacob, J. Opt. **14**, 063001 (2012).
22. E. E. Narimanov and A. V. Kildishev, Nat. Photonics **9**, 214 (2015).
23. M. M. Choy and R. L. Byer, Phys. Rev. B **14**, 1693 (1976).
24. H. Vanherzeele and J. D. Bierlein, Opt. Lett. **17**, 982 (1992).
25. R. Matsushima, N. Tanaka, O. Sugihara, and N. Okamoto, Chem. Lett. **30**, 200 (2001).
26. A. A. High, R. C. Devlin, A. Dibos, M. Polking, D. S. Wild, J. Perczel, N. P. de Leon, M. D. Lukin, and H. Park, Nature **522**, 192 (2015).
27. A. J. Hoffman, L. Alekseyev, S. S. Howard, K. J. Franz, D. Wasserman, V. A. Podolskiy, E. E. Narimanov, D. L. Sivco, and C. Gmachl, Nat. Mater. **6**, 946 (2007).
28. Y. Li, S. Kita, P. Munoz, O. Reshef, D. I. Vulis, M. Yin, M. Loncar, and E. Mazur, Nat. Photonics **9**, 738 (2015).